POLISH MARITIME RESEARCH 2 (118) 2023 Vol. 30; pp. 76-84
10.2478/pomr-2023-0023

GUIDED WAVES IN SHIP STRUCTURAL HEALTH MONITORING – A FEASIBILITY STUDY

Emil Roch [1*]
Beata Zima [1]
Krzysztof Woloszyk [1]
Yordan Garbatov [2]
[1] Gdańsk University of Technology, Poland
[2] Universidade de Lisboa, Portugal

* Corresponding author: *emil.roch@pg.edu.pl (Emil Roch)*

ABSTRACT

Ships and offshore structures operate in a severe corrosion degradation environment and face difficulty in providing long-lasting corrosion protection. The Classification Societies recommend regular thickness measurements leading to structural component replacements, to ensure structural integrity during service life. The measurements are usually performed using ultrasonic thickness gauges and such an approach requires multiple measurements of the corroded structural components. Otherwise, the collected data are insufficient to precisely assess the corrosion degradation level. This study aims to perform numerical and experimental analyses to verify the use of guided ultrasonic waves in defining the corrosion degradation level of the corroded structural components of a ship. The study incorporates the fundamental antisymmetric Lamb mode, excited by piezoelectric transducers attached at the pre-selected points on stiffened panels, representing typical structural ship components. The specimens are exposed to accelerated marine corrosion degradation, the influence of the degree of degradation on the wave time of flight being analysed. The study indicates that guided waves are a promising approach for diagnosing corroded structural components. The signals characterised by a high signal-to-noise ratio have been captured, even for relatively long distances between the transducers. This proves that the proposed approach can be suitable for monitoring more extensive areas of ship structures by employing a single measurement.

Keywords: Corrosion, Guided Waves, Non-destructive Testing, Ship Structures

INTRODUCTION

The current recommendations of the International Association of Classification Societies (IACS) specify the number of gauge measurements as being three per plate in maritime structures. Det Norske Veritas guidelines [1], based on the IACS requirements [2], recommend increasing the measures for more severe corrosion found in the investigated area and additional surveys when pitting corrosion is observed. However, those gauged measurements often do not provide enough information due to the high non-regularity of the geometry of corroded structural components [3], introducing a high level of uncertainty, and they do not provide enough information to analyse the severity level of corrosion degradation. Therefore, there is a need to develop alternative methods that could be more effective and inexpensive and allow for the monitoring of significant areas during a single measurement.

The guided wave propagation approach has recently attracted significant attention from researchers as a promising tool for non-destructive diagnostics. Due to the ability of the guided wave to travel long distances with insignificant amplitude reduction and their high sensitivity to defects, they are commonly used

for diagnostics in different industrial applications. For this purpose, the arrays of piezoelectric transducers are mounted on the surface of the tested structure or are embedded directly into the structure. They are used for data collection and generating mechanical guided waves (GW) [4, 5].

Some algorithms are dedicated to the detection, localisation and size estimation of various damage types, such as localised damages [4], debonding [6], deterioration of the structural parameters [7], etc. Special attention was paid to the non-destructive evaluation of the corrosion degradation level, as it is one of the most common degradation types of structures subjected to aggressive environmental conditions. Pitting and general corrosion were recently investigated by [7–14]. The method of corrosion pit detection and visualisation using the dispersion curve regression method was proposed by Tian et al. [9]. Ervin and Reis investigated the case of general corrosion of steel reinforcing bars embedded in concrete [10, 11]. Pulse-echo and pulse transmission methods were used by Sharma and Mukherjee [12] to monitor the corrosion process of the reinforcing bar. Moustafa et al. [13] proposed a method to evaluate the corrosion level in post-tensioned systems based on the fractal analysis of guided ultrasonic waves. The normalised acoustic nonlinearity parameter of the second and third harmonics was incorporated by Ding et al. [7], to evaluate the level of corrosion degradation. Laser-induced guided waves were used to estimate the corrosion pit size, location, and depth by Gao et al. [8].

The thickness reduction caused by corrosion degradation is currently measured using an ultrasonic gauge, which is time-consuming. Several studies have proved the potential of guided waves in non-destructive diagnostics of corrosion impact. Precise measurements of corroded element geometry are possible using other methods, such as photogrammetry or laser scanning. Nevertheless, those methods are expensive and challenging to use in the case of ship hull thickness measurements. Also, both sides of the plate need to be scanned and, thus, additional problems might occur because of the permanent deflection, buckling or residual post-welding stresses. Guided wave-based methods may increase the efficiency of the measuring process and reduce the associated costs of the time-consuming traditional inspections.

This study aims to perform numerical and experimental feasibility analyses to evaluate the use of guided ultrasonic waves in estimating the degradation level of corroded stiffened panels as a part of ship hulls. Contrary to our previous studies [15, 16], where only distances of approximately 300 mm were investigated, this proves the possibility of using the guided waves on longer distances (up to 1250 mm), which is crucial for increasing the effectiveness and reducing the total cost of the state assessment. Previous work was devoted to analysing the possibility of monitoring plate corrosion degradation. The current study is the next step towards a more realistic scenario of inspecting a ship's structural components when the whole of the plates, with complex geometry and additional obstacles like stiffeners, need to be tested. The study incorporates a fundamental antisymmetric Lamb mode excited by piezoelectric transducers attached to pre-selected locations on stiffened panels. Before non-destructive testing, the stiffened panels are exposed to accelerated natural marine corrosion in a specially designed and prepared corrosion tank.

CORRODED SAMPLE SET-UP

Experimental testing of guided wave propagation was conducted on mild steel specimens with an initial plate thickness of t = 6 mm. The geometry of the specimens is presented in Fig. 1. These stiffened plates (plates reinforced by stiffeners) are typical structural components of ship hull structures.

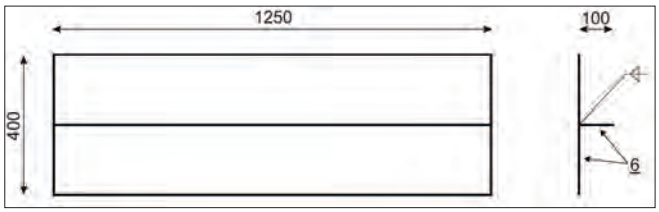

Fig.1. Intact specimen geometry (dimensions in mm)

The experiment includes one intact sample and three specimens with different degrees of corrosion degradation (*DoD*). The *DoD* is considered as the percentage loss of the initial mass of the specimen (m_{intact}) which is reduced due to corrosion degradation (mass after corrosion – $m_{corroded}$):

$$DoD = \frac{m_{intact} - m_{corroded}}{m_{intact}} \cdot 100\% \quad (1)$$

Therefore, only the specimen's mean thickness loss is captured, without considering the irregular character of the corrosion damage. Corrosion of the specimens was accelerated in a specially designed tank with corrosion process parameters: salinity 3.5%, temperature 55°C and increased dissolved air (fully saturated conditions). The *DoD* achieved were 12% (specimen *c*12) and 24% (specimen *c*24) and were taken from mass measurements. The mean thickness reduction, calculated based on mass reduction, is presented in Table 1. Thickness measurements were also performed using a micrometre screw along both long edges. The thickness measurements were made alongside the edges because of the transducer configuration, which will be presented later in this paper, and the mean thicknesses are presented in Table 1. Finally, ultrasonic thickness gauge measurements were also performed on the plates, resulting in a thickness map, as shown in Figure 2. Due to the significant difference between UT measurements and micrometre screws, UT measurements were only used to represent corrosion irregularity.

Tab. 1. DoD and mean specimen thickness.

Specimen	*DoD* [%]	Path (as seen in Fig. 7)	Mean thickness based on *DoD* [mm]	Mean thickness on edge [mm]
intact	0	–	6.00	6.00
c12	12	I	5.28	5.34
		II		5.46
c24	24	I	4.56	4.76
		II		4.98

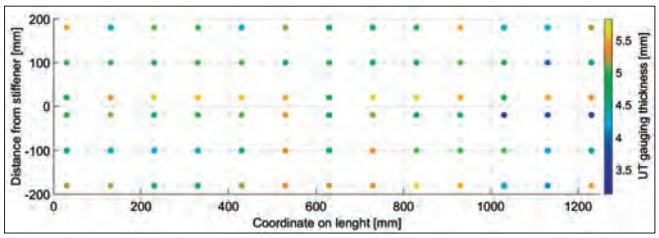

Fig. 2. Plate thickness distribution, specimen c24, UT gauging

Figures 3 and 4 present photos of selected specimens. Figure 3 shows a close-up view of the intact and corroded plate surface. On the intact plate, the surface was as it arrived from the steel mill. The corroded surface was dried out and so the authors removed loose corrosion products and dusted up the surface. Figure 4 presents a stiffener side view on the *c*12 sample, with magnifications on given parts of the plate. Apart from specimen markings, there are visible white dots on the sample, indicating places where UT gauging was performed.

Fig. 3. Plate surface close-up. Left: intact plate. Right: c24 plate corroded and cleaned from corrosion products

Fig. 4. Sample c12 (12% DoD): stiffener side view with close-ups of surface.

BACKGROUND OF GUIDED WAVES

One of the essential features of guided waves is their dispersive nature. The relationship between their velocity and the number of wave modes is usually presented as a dispersion curve, which can be traced by solving dispersion equations. For the plate-like structures, the dispersion relationships were formulated by Lamb [17]. Thus, the waves are called Lamb waves. Two Lamb wave families can be distinguished: antisymmetric (Eq. (2)) and symmetric (Eq. (3)). The dispersion relations are as follows:

$$\frac{tan(qd)}{tan(pd)} = \frac{(k^2-q^2)^2}{4k^2pq} \quad (2)$$

$$\frac{tan(qd)}{tan(pd)} = \frac{4k^2pq}{(k^2-q^2)^2} \quad (3)$$

The parameters d and k indicate the plate thickness and the wavenumber, respectively, while q and p depend on longitudinal and transverse wave velocities in an infinite medium. Based on the equations, the curves illustrating the relationships between velocity and excitation frequency can be traced, as shown in Fig. 5.

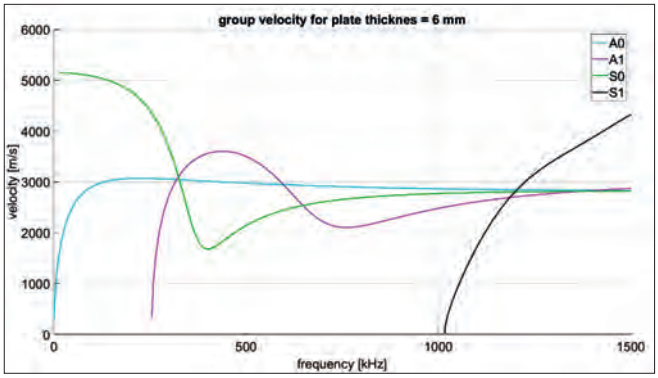

Fig. 5. Group velocity against frequency for 6 mm steel plate (A-antisymmetric, S-symmetric mode)

Piezoelectric transducers were mounted at pre-selected points on the plate surface to generate guided waves. Because the transducers were attached to the plate surface, and the excitation applied perpendicular to it, antisymmetric modes were mainly excited. The significant difference between velocities (for the antisymmetric A0 and S0 modes for frequencies incorporated in the experimental tests, the velocity of S0 mode is higher than A0 mode by about 2000 m/s for a frequency of 140 kHz) result in the mode family being easily recognised, based on the difference in the time of flight. The scheme of deformation forms an antisymmetric wave (A0), as seen in Fig. 6.

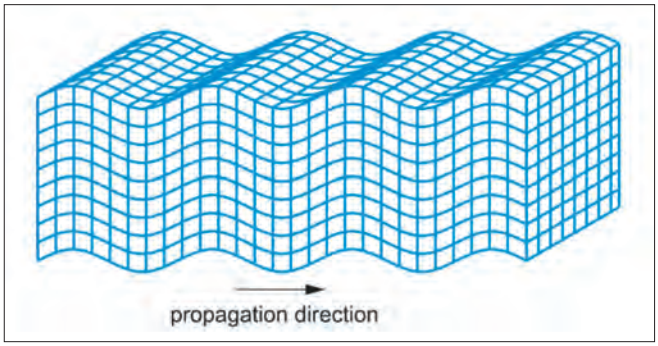

Fig. 6. Deformation form of antisymmetric wave propagation

In the presented paper, we use the commonly known guided wave feature, i.e. its velocity strongly depends on the plate thickness. Therefore, if the wave propagation velocity is known, we can determine the average thickness of the specimen alongside the propagation path. Eq. (2) was solved to demonstrate the velocity-thickness dependency and a good curve representing this relationship, for a frequency of 140 kHz, was plotted (Fig. 7).

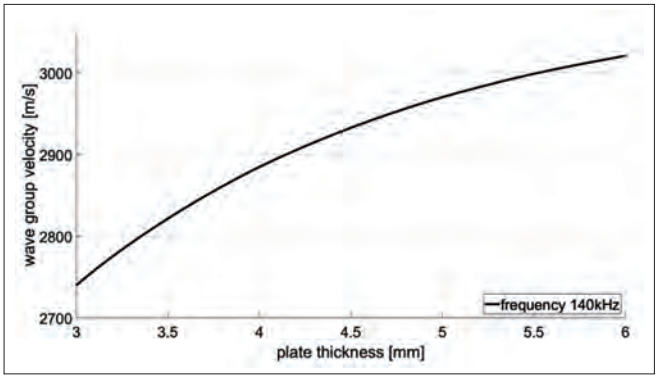

Fig. 7. Antisymmetric group wave velocity to plate thickness curve

Since the distance between measurement points is constant, the change in the flight time may be associated with corrosion degradation and thickness reduction. This assumption is the basis of the presented analysis. Later in the paper, the thickness reduction will be estimated, based on the time of flight (ToF), which is the time needed to travel from an actuator to the sensor. Therefore, for an exemplary frequency of 140 kHz, the relationship between the ToF measured on the distance of 1250 mm, which is the length of the considered ship hull structural element, is presented in Fig. 8. It should be noted that the dispersive equations (Eq. (2) and (3)) are nonlinear and the ToF-thickness relationship is also nonlinear.

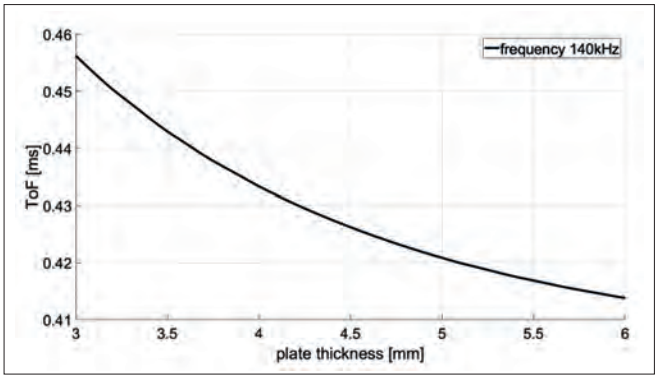

Fig. 8. Antisimetric 140 kHz wave ToF in different plate thicknesses at 1250 mm distance

MATERIALS AND METHODS

ANALYSED STRUCTURAL COMPONENTS

Piezoelectric transducers were mounted in plate corners as pairs, the first for path I and the second for path II. Transducers were attached on the right hand corner of the plate by using special wax as a coupling medium. Transducer positions and the geometry of the tested plate can be seen in Fig. 9.

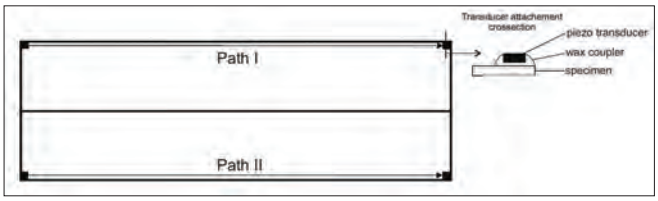

Fig. 9. Transducer locations and paths (left) and cross-section of transducer (right)

EXPERIMENTAL SET-UP AND TRANSDUCER CONFIGURATIONS

Transducers were connected to a wave generator, amplifier, and oscilloscope, as presented in Fig. 10. The signal measured from a series of the same signals was then averaged at an oscilloscope, filtered using an oscilloscope-integrated low pass filter (with double base cut-off frequency), and stored as a voltage-time relationship.

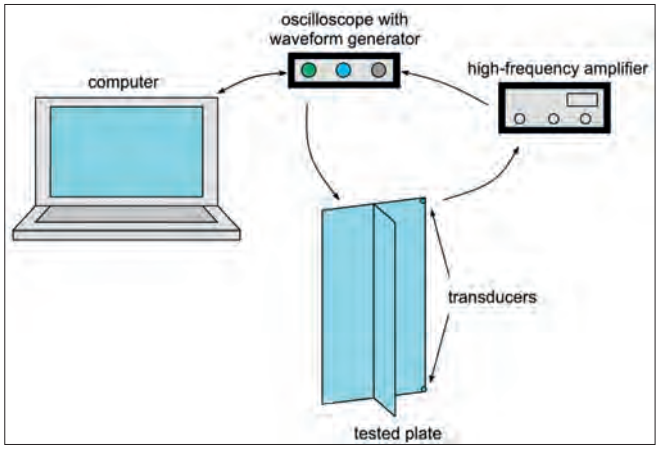

Fig. 10. Guided wave experimental set-up.

Two paths were investigated in the study, both along the longer sides of the plates. The signal generated by the wave generator was a packet consisting of a five-cycle sine modulated by the Hanning window, as presented in Fig. 11.

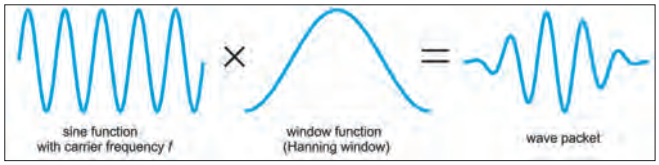

Fig. 11. Windowing sine signal using the Hanning window

In the study, the piezoelectric transducers were attached near the corners of the plate for two reasons. First, fewer reflections provide a cleaner, more readable signal; second, energy only disperses at a quarter of the circle instead of the entire circular wavefront. Thus, the signal energy was about four times higher than in the case of attachment in the middle part of the plate [18]. Parts of the ship structure have free edges; however, applying the method to plates limited by stiffeners or girders should be possible. It is expected that the signal-to-noise ratio might be lower but the basic operating principle should be kept the same.

SELECTION OF EXCITATION PARAMETERS

In the first step, the sensitivity analysis aimed at determining the influence of excitation frequency on signal amplitude, was carried out to investigate corroded plates. A waterfall chart is presented in Fig. 12, registering signals for frequencies in the range 60-300 kHz, with a step of 20 kHz. It can be seen that the amplitude of the incident wave significantly decreases for a frequencies lower than 100 kHz and higher than 160 kHz.

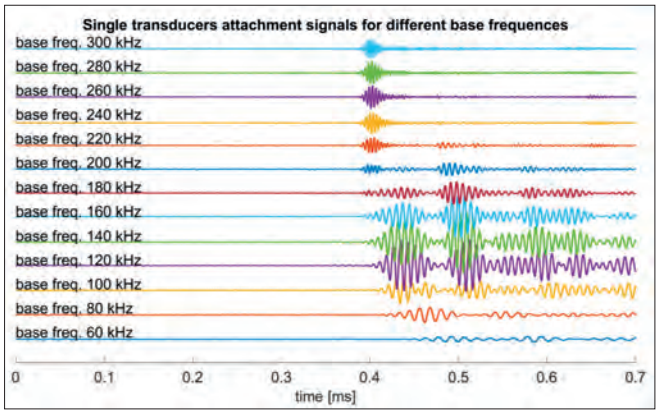

Fig. 12. Waterfall chart of signal received for different base frequencies.

Maximal amplitudes of the received signals were registered and are presented in Fig. 13. The highest amplitudes of the incident waves lead to the highest signal-to-noise ratios and were achieved for the frequency 140 kHz. The final data were only collected and analysed for this frequency because it provided the clearest and the most readable signals.

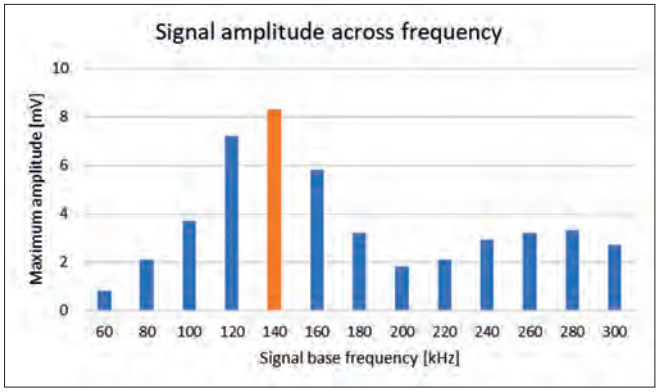

Fig. 13, Column chart of registered amplitudes for base frequencies.

NUMERICAL MODEL

Numerical simulations were performed using commercial FEM (finite element method)-based software (Abaqus) [19], to demonstrate and recreate experiments on the wave propagation phenomena in the stiffened plate. The dynamic/Explicit module was used to accurately model mechanical wave propagation. Guided waves were simulated in intact and corroded specimens modelled as a constant-thickness shell structure. Four node shell elements were applied with reduced integration (S4R). A convergence study preceded the numerical analysis, to determine the element size. Finally, each element had the same dimensions (1 mm x 1 mm). The transient wave propagation problem was solved with a 10-7 s time step, adjusted according to CFL (Courant–Friedrichs–Lewy) conditions [20] related to frequency and wavelength. The mechanical properties were a Poisson's ratio of 0.3 and a material density equal to 7800 kg/m^3, which was established based on previously conducted experimental destructive tests performed on specimens of the same steel. An elastic modulus of 188.5 GPa was calculated non-destructively, based on the Lamb equation for the intact plate. Because Poisson's ratio has a relatively small influence on the shape of the dispersion curves, only elastic modulus was considered during the calibration procedure and curve fitting. The geometry was consistent with the dimensions of the intact specimen presented in Fig. 1. The simulations were made for plate thicknesses taken as average thickness from the measurements with the use of micrometer, of each path (see Fig. 9).

RESULTS AND DISCUSSION

VISUALISATION OF WAVE PROPAGATION IN SHIP STRUCTURE

Figure 14 presents the numerical simulation results in snapshots collected for selected time instants. After wave excitation at the corner of the plate, the circular wavefront was observed propagating within the structure. The material is assumed to be isotropic and homogeneous, which means that the propagation velocity is the same in each direction. The presence of the stiffener triggers additional reflections, affecting the wave propagation patterns. As a result, surface waves (Rayleigh waves) are observed, propagating along the plate edges. Therefore, the diagnostic procedures dedicated to ship structures should consider the more complex geometry and the presence of additional waves affecting registered signals.

Even though the numerical model did not consider thickness variability along the propagation path, and the thickness was assumed to be constant, the influence of modelled corrosion degradation is visible in visualisation. The wave propagates with a higher velocity in the intact plate (see Fig. 14, t = 0.46 ms). The difference in wave velocity can be explained by the dispersive character of guided waves (see Eq. (2) and (3)).

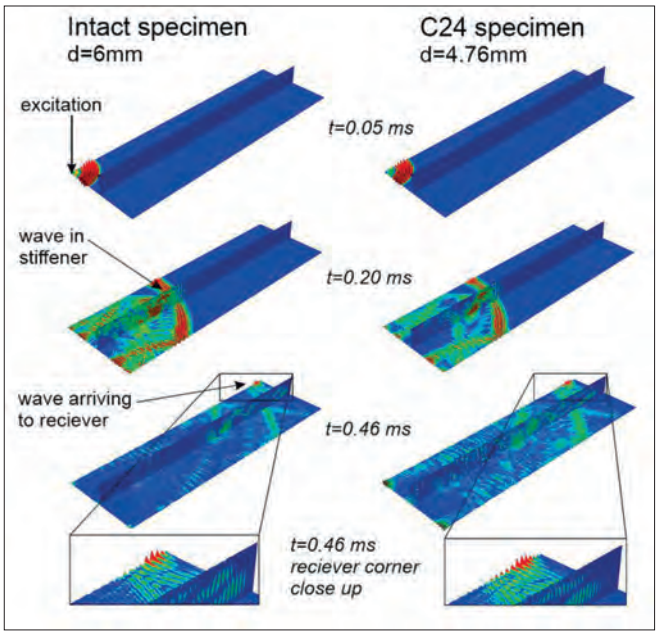

Fig. 14. Visualisation of wave propagation – deformation: intact specimen and specimen characterised by DoD of 24%

EXPERIMENTAL RESULTS

Figure 15 shows the received signal from two measurements, both for the intact plate but at opposite sides. Since the transducer's ability to actuate and receive a signal depends on the attachment and the wax used for transducer mounting, signal amplitude cannot be compared directly. To make signals possible to compare, they were all normalised to a 1V amplitude at the peak of the first packet received after about 0.4-0.5 ms.

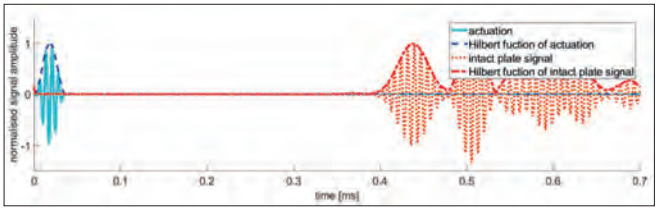

Fig. 15. The comparison of the signals measured alongside both edges of the intact plate

The envelopes of the signals were determined by using Hilbert transform to interpret and present signals more clearly. Figure 16 presents the actuation signal, registered signal, and Hilbert transforms, as well as the interpretation of the ToF, which is used in further analysis. This study measures the ToF as the peak-to-peak value between the actuation and registered signals. As the lengths of both paths are equal, ToF can be used for group velocity comparison.

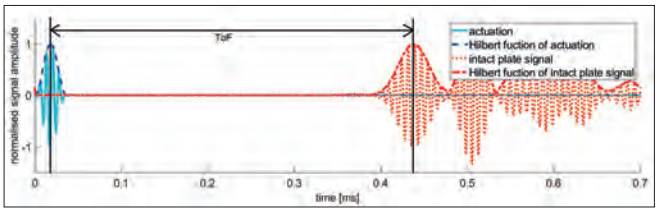

Fig. 16. Excitation and received signal for intact sample, excitation 140 kHz

Figures 17 and 18 show the Hilbert transforms of the normalised signal received for intact and corroded specimens. All signals were triggered in a similar way, i.e. for the time $t = 0$ ms. Figure 17 presents the results for the first path of all three plates. As predicted by theoretical analysis, the signal travelled with a higher velocity in an intact plate. Next, the waves propagating in plates *c*12 and *c*24 were registered.

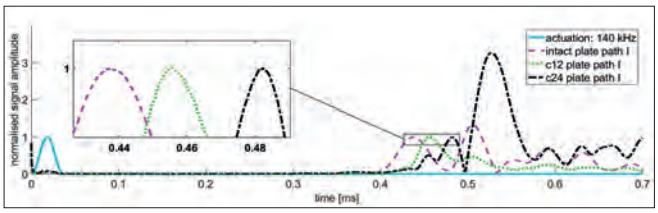

Fig. 17. Hilbert transforms of actuation and signals received at path I

Figure 18 presents the results for the second path alongside the opposite edge. As path I, the wave travelled with the highest velocity in an intact plate. The clear relationship between increasing ToF and the degree of degradation is demonstrated in Fig. 18. For comparison, the ToF for all registered signals was determined and is summarised in Table 2.

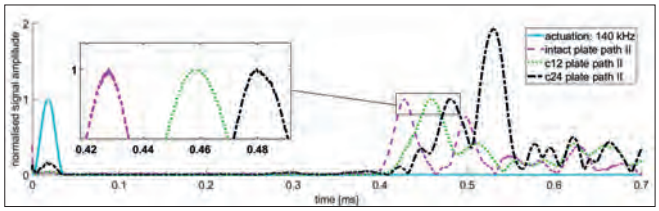

Fig. 18. Hilbert transforms of actuation and signals received at path II

Tab. 2. Values of Time of Flight (ToF) measured at Hilbert transform peak [ms]

Specimen	Path	Mean thickness on edge [mm]	ToF [ms]
intact	I	6.00	0.419
	II	6.00	0.409
c12	I	5.34	0.437
	II	5.46	0.441
C24	I	4.76	0.463
	II	4.98	0.461

NUMERICAL RESULTS

The results of the FEM simulations, in the form of Hilbert transforms of registered signals, are presented in Fig. 19. The thickness chosen to calculate ToF with FEM corresponds with the mean path thickness from micrometer screw measurements. The same relation between ToF and thickness can be observed: the smaller the plate thickness, the greater ToF.

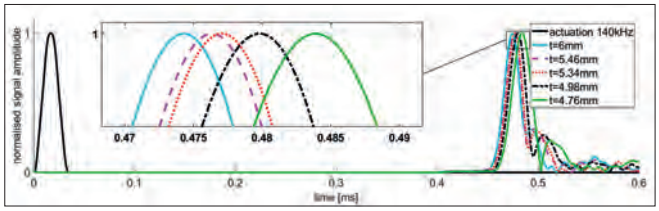

Fig. 19. Hilbert transform of received signals from FEM analysis: both for intact and 24% DoD plate

Figure 20 presents the experimental and numerical ToFs. FEM values were calculated based on the mean thickness of the path from the micrometer. It can be seen that all ToFs for the FEM-tested plates are more significant than in the experimental plates. This can be explained by the fact that the constant average thickness was adopted in the numerical model, while the corroded surface was irregular in the real case. However, in both cases, the same decreasing trend is noted.

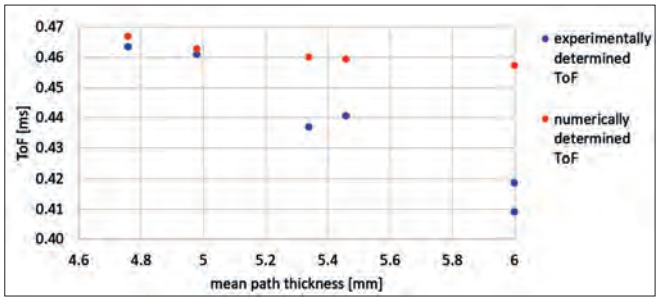

Fig. 20. Twenty FEM results compared with experimental results

COMPARISON OF EXPERIMENTAL AND THEORETICAL RESULTS FROM LAMB EQUATIONS

As previously mentioned, the relationship between ToF and the plate thickness is strongly nonlinear and requires the solving of dispersion equations. Based on the experimentally determined material parameters, the theoretical curve representing the thickness-ToF relationship was calculated for an incorporated frequency of 140 kHz and compared with experimental results (Fig. 21).

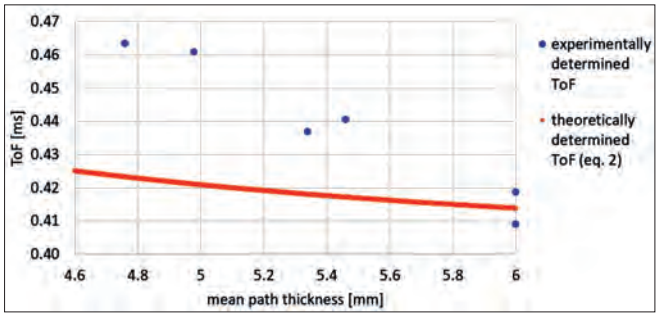

Fig. 21. ToF to thickness curve from equations in front of ToF measured in the experiment

In the last stage, an algorithm was developed in the MATLAB environment, to fit the theoretical curve to the experimental results. The theoretical curve was calculated based on solving Eq. (2), using material parameters from the paragraph describing the numerical model. This was used to fit the dispersion curve based on the regression analysis, using the least square method. The algorithm considers plate thickness and the systematic error of the ToF measurements. Because several approaches for ToF determination give slightly different results, it was assumed that the results could be burdened with some systematic errors. Moreover, the delay resulting from signal transmission between the components of the experimental set-up might also affect the ToF values. Based on the regression analysis results, the error value was estimated at 0.036 ms.

The discrepancies between experimental and numerical results may also result from the differences between the material parameters determined using the fitting Lamb equation to the experimental results. The difference between the actual specimen's average thickness, alongside the propagation paths and the thickness obtained by solving the inverse problem using Lamb equations, was checked and calculated. The inverse calculation was based on the wave propagation velocity for a given average path thickness. The final inaccuracy was calculated as 2.8 mm. This means that, based on the non-destructive results and fitting curve procedure, the plate is thinner by 2.8 mm .

The results of the curve fitting (after considering the inaccuracies) that translates the curve by translation vector [ToF; d] = [-0.036 ms; 2.8 mm], are presented in Fig. 22. The solid curve represents the theoretically determined thickness-ToF relationship, while experimental results are marked with green markers. It can be seen that the experimental and theoretical results coincide well with each other. The absolute average difference between experimental results and the fitted curve equals 0.005 ms, and the maximum difference between observed ToF values equals 0.054 ms.

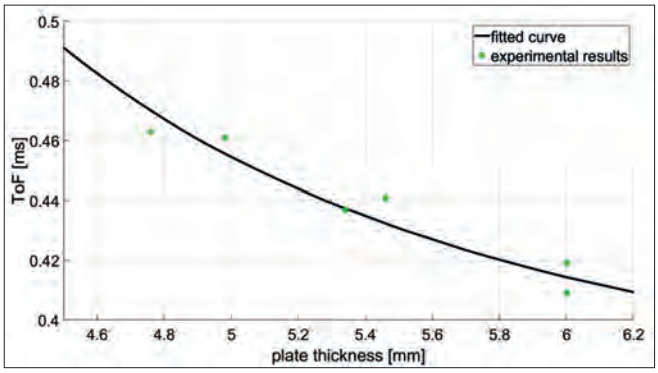

Fig. 22. Translated curve fitted to experimental results, non-translated curve for reference.

CONCLUSIONS

This study analysed the possibility of applying guided waves to the health monitoring of a ship's structural components subjected to corrosion degradation. The correlation between ToF and mean plate thickness can be easily observed in naturally accelerated corroded plates. This ensures that the guided wave dispersion might be used to estimate the mean value of the thickness loss of the plate, which was proven in many previous papers. However, it was observed that guided waves could easily travel significant distances on the plates, which is promising when analysing the large-scale structural components typically found in ship structures. The experiments presented were performed on a simpler geometry. However, they can be performed for other, more complex geometries. Signals would differ due to different distances or additional reflections. As a feasibility study, the paper proves the concept of structural health monitoring based on the time of flight. Testing this possibility was also important in the context of the reliability of the wave-based method. It could be observed that even a relatively high degradation level was associated with insignificant differences in the ToF. In the case of short distances, the difference would be invisible, and the state assessment would be more challenging to perform.

In the next stage, we could observe the influence of the inaccuracies of ToF determination, as well as the complex geometry of the corroded plates. Developed FEM models, theoretical dispersion curves and experimental results do not overlap perfectly. It should be noted that FEM and Lamb's curves are biased. After determining the translation vector, the results were matched with high accuracy. The main source of the discrepancies between numerical, theoretical and experimental results is an incorrect assumption commonly applied in the literature about the reduced constant thickness plate. In real cases, the corroded plates are characterised by irregular surfaces, while thickness variability entails variable velocity alongside the propagation path. The second important aspect, which should be considered in further investigations, is the complex structure of the corroded plate. Because corrosion products and coatings differ in terms of their parameters, the plate should be regarded

as a multi-layered structure, with layers varying in thickness and material parameters.

The next problem discussed in the paper concerned the influence of material parameters (elastic modulus) on the theoretical reference curve. A solution for this might be the opportunity to calibrate measurement techniques on the intact element. In this study, we have not compared the results for the same specimen but for various degradation levels, i.e. several specimens varying in *DoD*. In the case of monitoring the same element, the influence of inaccuracies in material parameter estimation would have a much smaller impact on the final results.

To understand the wave propagation phenomenon in multi-layered plate-like structures with variable thickness, more samples need to be tested, with a detailed knowledge of the surface topography, determined with the support of photogrammetry or CMM, and defined by statistical parameters. It is worth mentioning that, in the initial stages of introducing the method to diagnosing the construction, support from the mentioned methods may still be necessary. However, such an approach would allow for the further development of a mathematical model, describing the relationship between average wave velocity and surface parameters.

The paper demonstrates the possibilities of using guided waves, even for the more complex specimens. The tested plates were stiffened with an additional web in the middle parts. The incident wave was easily identified despite the additional obstacles and the ToF was calculated. This is essential in the ToF-based methods because, very often, the interference of several different wave packets efficiently identifies the first peak and, consequently, estimates the ToF. The results presented here prove that the sensor network can be set in a way that facilitates the non-destructive testing procedure.

Future work should also consider comprehensive research on the wave's ability to overcome obstacles, such as stiffeners or deep girders. Also, research about plate measurements reinforced by stiffeners and deep girders is necessary for possible practical applications using wave-guided methods.

A potential problem with the in situ application of this method is the necessity to specify the Young modulus, which strongly influences group speed.

ACKNOWLEDGEMENTS

The research was carried out within project No. 2021/43/D/ST8/00786, financed by the National Science Centre, Poland. Abaqus calculations were carried out at the Academic Computer Centre in Gdańsk.

The third author would like to thank for the support of the Foundation for Polish Science (FNP).

REFERENCES

1. DNV GL, *CLASS GUIDELINE Ultrasonic thickness measurements of ships*, 2016. [Online]. Available: http://www.dnvgl.com.
2. ACS, "IACS UR Z7," *UR Z7 Hull classification surveys*, 2020.
3. K. Woloszyk, Y. Garbatov, and J. Kowalski, "Indoor accelerated controlled corrosion degradation test of small and large-scale specimens," *Ocean Engineering*, vol. 241, p. 110039, Dec. 2021, doi: 10.1016/j.oceaneng.2021.110039.
4. B. Zima and R. Kędra, "Debonding Size Estimation in Reinforced Concrete Beams Using Guided Wave-Based Method," *Sensors*, vol. 20, no. 2, p. 389, Jan. 2020, doi: 10.3390/s20020389.
5. B. Zima and M. Rucka, "Guided waves for monitoring of plate structures with linear cracks of variable length," *Archives of Civil and Mechanical Engineering*, vol. 16, no. 3, pp. 387–396, May 2016, doi: 10.1016/j.acme.2016.01.001.
6. A. Farhidzadeh and S. Salamone, "Reference-free corrosion damage diagnosis in steel strands using guided ultrasonic waves," *Ultrasonics*, vol. 57, no. C, pp. 198–208, Mar. 2015, doi: 10.1016/j.ultras.2014.11.011.
7. X. Ding, C. Xu, M. Deng, Y. Zhao, X. Bi, and N. Hu, "Experimental investigation of the surface corrosion damage in plates based on nonlinear Lamb wave methods," *NDT & E International*, vol. 121, p. 102466, Jul. 2021, doi: 10.1016/j.ndteint.2021.102466.
8. T. Gao, H. Sun, Y. Hong, and X. Qing, "Hidden corrosion detection using laser ultrasonic guided waves with multi-frequency local wavenumber estimation," *Ultrasonics*, vol. 108, p. 106182, Dec. 2020, doi: 10.1016/j.ultras.2020.106182.
9. Z. Tian, W. Xiao, Z. Ma, and L. Yu, "Dispersion curve regression – assisted wideband local wavenumber analysis for characterising three-dimensional (3D) profile of hidden corrosion damage," *Mech Syst Signal Process*, vol. 150, p. 107347, Mar. 2021, doi: 10.1016/j.ymssp.2020.107347.
10. B.L. Ervin and H. Reis, "Longitudinal guided waves for monitoring corrosion in reinforced mortar," *Meas Sci Technol*, vol. 19, no. 5, p. 055702, May 2008, doi: 10.1088/0957-0233/19/5/055702.
11. B.L. Ervin, D.A. Kuchma, J.T. Bernhard, and H. Reis, "Monitoring Corrosion of Rebar Embedded in Mortar Using High-Frequency Guided Ultrasonic Waves," *J Eng Mech*, vol. 135, no. 1, pp. 9–19, Jan. 2009, doi: 10.1061/(ASCE)0733-9399(2009)135:1(9).
12. S. Sharma and A. Mukherjee, "Longitudinal Guided Waves for Monitoring Chloride Corrosion in Reinforcing Bars in Concrete," *Struct Health Monit*, vol. 9, no. 6, pp. 555–567, Nov. 2010, doi: 10.1177/1475921710365415.
13. A. Moustafa, E.D. Niri, A. Farhidzadeh, and S. Salamone, "Corrosion monitoring of post-tensioned concrete structures

using fractal analysis of guided ultrasonic waves," *Struct Control Health Monit*, vol. 21, no. 3, pp. 438–448, Mar. 2014, doi: 10.1002/stc.1586.

14. L. Xiao, J. Peng, J. Zhang, Y. Ma, and C.S. Cai, "Comparative assessment of mechanical properties of HPS between electrochemical corrosion and spray corrosion," *Constr Build Mater*, vol. 237, p. 117735, Mar. 2020, doi: 10.1016/j.conbuildmat.2019.117735.

15. B. Zima, K. Woloszyk, and Y. Garbatov, "Experimental and numerical identification of corrosion degradation of ageing structural components," Ocean Engineering, vol. 258, p. 111739, Aug. 2022, doi: 10.1016/j.oceaneng.2022.111739.

16. B. Zima, K. Woloszyk, and Y. Garbatov, "Corrosion degradation monitoring of ship stiffened plates using guided wave phase velocity and constrained convex optimisation method," *Ocean Engineering*, vol. 253, p. 111318, Jun. 2022, doi: 10.1016/j.oceaneng.2022.111318.

17. Z. Su, L. Ye, and Y. Lu, "Guided Lamb waves for identification of damage in composite structures: A review," *J Sound Vib*, vol. 295, no. 3–5, pp. 753–780, Aug. 2006, doi: 10.1016/j.jsv.2006.01.020.

18. B. Zima and R. Kędra, "Detection and size estimation of crack in plate based on guided wave propagation," *Mech Syst Signal Process*, vol. 142, p. 106788, Aug. 2020, doi: 10.1016/j.ymssp.2020.106788.

19. Smith M., *ABAQUS/Standard User's Manual*. Dassault Systèmes Simulia Corp, 2009.

20. Courant R., Friedrichs K, and Lewy H., "On the partial difference equations of mathematical physics," *IBM*, no. 11, pp. 215–234, 1967.